Dielectric properties of solids in the regular and split-charge equilibration formalisms

Razvan A. Nistor and Martin H. Müser*
Department of Applied Mathematics, University of Western Ontario, London, Ontario, Canada N6A 5B7
(Received 9 December 2008; revised manuscript received 18 February 2009; published 24 March 2009)

We investigate the generic dielectric properties of solids in the split-charge equilibration (SQE) formalism, which contains the regular charge equilibration (QE) method as a limiting case, but augments it with a bond hardness term. It is shown that QE always mimics ideal conductors, while any positive bond hardness used in SQE turns the solid into a dielectric. Crystals with simple cubic and rocksalt structure are considered explicitly. For these symmetries, we solve the continuum limit of the SQE formalism analytically. As a result, we provide simple analytical expressions for how dielectric constant and penetration depth of the electrostatic field depend on atomic hardness, bond hardness, and lattice constant. This mapping may prove useful not only for force field parametrization but also for solving dielectric responses on coarse-grained scales. Successful comparison of numerical data to analytical solutions is made, including those containing discretization corrections.

DOI: 10.1103/PhysRevB.79.104303 PACS number(s): 77.22.−d, 02.70.Ns, 34.70.+e, 34.20.Cf

I. INTRODUCTION

Assigning meaningful atomic charges to atoms is an important aspect of force field development as long-range interactions crucially depend on the charge of an atom.[1–3] This task is difficult when dealing with heterogeneous media, such as interfaces between silicon and silica, as one cannot know what effective charge to give to atoms near the interface prior to a simulation. Similar comments apply to many other chemically heterogeneous systems, which is why there is a broad interest in assigning atomic charges that reasonably reproduce the electric fields generated by the systems of interest.

The schemes of assigning atomic charges can be roughly divided into two categories: atom-based and bond-based approaches. In the atom-based methods,[4,5] which are also known as charge equilibration (QE) methods, partial charges are chosen such that they minimize the potential energy function V_{pot},

$$V_{\mathrm{pot}} = \sum_i \left(\frac{\kappa_i}{2} Q_i^2 + \chi_i Q_i \right) + V_C, \tag{1}$$

typically under the constraint that the net charge is neutral. Here, Q_i is the charge of atom i, κ_i and χ_i are its hardness and electronegativity, respectively, and V_C is the (potentially screened) Coulomb interaction between the charges plus their coupling to electrostatic potentials originating from additional sources. An attractive aspect of QE methods is that their functional form can be motivated from density-functional theory (DFT) arguments.[4,6,7] Moreover, the values for κ and χ can be determined from measurable atomic parameters, i.e., electronegativity and ionization potential. Thus these parameters should be transferable in principle.

One disadvantage of the QE method is that noninteger charges can be transferred between two atoms across large distances; e.g., hydrogen and fluorine would be assigned partial charges even if the chemical bond of the HF molecule was broken. This charge transfer is in contrast to the observation that both atoms become neutral at large separation as the ionization potential of hydrogen exceeds the electronegativity of fluorine. The ability of atom-based QE methods to invoke such nonlocal charge transfer is responsible for the improper scaling of the polarizability of simple alkane chains with the degree of polymerization;[8,9] i.e., the dielectric response is automatically that of a conducting polymer. This result implies that condensed phases of QE systems are also conducting and that the electrostatic fields near the surfaces are parallel to the surface normal. Hence, QE methods will generally not give accurate approximations of electrostatic fields near dielectric clusters and solids because it ignores the two transverse components that tend to be present in the electrostatic fields produced by real dielectrics.

In newer atomic charge-transfer approaches, some but not all of the discussed problems have been cured. For example, in the quadratic valence-bond model (VBM) (Ref. 10) the electronegativity difference between two atoms is made distance dependent, thereby producing the correct dissociation limit of diatomic molecules.[11] However, a small externally imposed difference in the electrostatic potential, which could be due to a third particle, would still induce nonlocal charge transfer.[12] In the fluctuating charge model and generalizations thereof,[13,14] nonlocal charge transfer is suppressed by constraining the charge in individual molecules, which requires *ad hoc* assumptions on the bonding situation and makes it conceptually difficult to include bond breaking into the approach.

In order to remedy the nonlocal charge-transfer problem, bond-based descriptions were developed in which charge can only be transferred between two bonded atoms.[8,14] If the charge transferred from atom j and atom i is denoted by q_{ij}, then the net charge of atom i is

$$Q_i = \sum_j q_{ij}, \tag{2}$$

where $q_{ij}=-q_{ji}$. In bond-based approaches, the hardness is associated with the charges, q_{ij} transferred across a bond, rather than with the atoms. Thus, the term $\Sigma_i \kappa_i Q_i^2/2$ in Eq. (1) is replaced with $\Sigma_{ij} \kappa_{s,ij} q_{ij}^2$, where the sum runs over all bonds involving atoms i and j, and κ_s denotes the bond hardness. An advantage of pure bond-based descriptions is that κ_s can be made as distance dependent, whereby charge transfer across large distances can be suppressed. However, a pure

bond description loses the attractive feature of QE approaches that the parameters κ and χ are motivated from DFT. Moreover, the polarizability of alkane chains with the degree of polymerization exhibits the wrong scaling in the limit of small chains.[9]

Recently, the split-charge equilibration (SQE) approach was proposed, which combines the ideas of atom-based and bond-based approaches in one model. In its simplest or default variant, V_{pot} can be expressed as

$$V_{\text{pot}} = \sum_{i,j>i} \frac{\kappa_{s,ij}}{2} q_{ij}^2 + \sum_i \left(\frac{\kappa}{2} Q_i^2 + \chi_i Q_i \right) + V_C. \tag{3}$$

In this variant SQE retains the parameters κ and χ that are motivated from DFT but also includes the phenomenologically added bond hardness term, κ_s, which penalizes charge flow between two atoms. The SQE model can be parametrized to produce the correct dissociation limits of molecules by turning the bond hardness into a distance-dependent term,[12,15] and it shows more accurate scaling with the degree of polymerization than other charge equilibration schemes,[9] thereby remedying the problems associated with charge-transfer potentials mentioned so far. Lastly, the SQE approach contains the pure bond- and pure atom-type approaches as limiting cases by setting either the atomic or the bond hardnesses to zero, respectively. For these reasons, the SQE formalism is a promising avenue to accurately describe atomic charge transfer in classical force fields.

In this work, we wish to elucidate another advantage of the SQE method, namely, the ability to tune the dielectric response of a solid by turning on the pure bond hardness term in the formalism, without having to resort to reverse mapping schemes beforehand, such as reverse Monte Carlo.[16] Charge equilibration methods are usually parametrized for molecules in the gas phase. While the methodology has been applied to the condensed phases, in particular in molecular-dynamics simulations, we are not aware of an attempt to determine the two most important phenomenological dielectric materials constants, namely, the dielectric constant and the penetration depth, from the QE or SQE model parameters. It is the intention of this work to fill this gap. We will do this by a combination of analytical and numerical works; in particular, we investigate the dielectric response of a simple cubic and rocksalt lattice to an external field. This will be done by investigating the continuum limit of the SQE model, which can be solved analytically.

II. THEORY

In this section, we discuss the generic dielectric properties of our ordered one-component (simple cubic) and two-component (rocksalt) systems. To do this, we first calculate the expected charges for the sublattices of the rocksalt structure and discuss the stability of the solution as a function of the model parameters, which are the lattice constant, a, the Madelung constant, α_M, and the split-charge parameters. Next, we introduce notation required for the later analytical sections in which we derive the continuum limit of the SQE approach and its solution. Special attention is paid to the response of a dielectric solid in a capacitor geometry from which one can derive simple analytical expressions for the dielectric constant and the penetration depth. Our treatment will also include discretization corrections that move our treatment beyond the continuum limit.

Generalization to more complicated compositions and geometries can be made in a straightforward fashion, and therefore conclusions we draw on our very simple model systems should remain valid for other two-component structures. The main differences between simple and complex geometries would be that dimensionless factors in the equations would turn out differently for other crystal geometries and that coupling between next-nearest neighbors would lead to similar changes in wavelength-dependent properties as they do in problems related to lattice dynamics.

A. Atomic charges for the rocksalt structure

For a strictly period rocksalt crystal it is a straightforward procedure to calculate the atomic charges because each split charge is identical, except for a sign, i.e., $q_{ij} = \pm q_s$, where we chose q_s to be positive. In the rocksalt structure, where each atom has six neighbors of opposite charge, the atomic charges are $Q_i = \pm 6 q_s$, depending on the ion type. If α_M denotes the Madelung constant and $N_n = 6$ is the number of nearest atoms, then the energy per atoms v is given by

$$v = \frac{N_n}{4} \kappa_s q_s^2 + \frac{1}{2} \kappa (N_n q_s)^2 - \frac{\alpha_M}{4\pi\epsilon_0} \frac{(N_n q_s)^2}{a} \pm \frac{\Delta\chi}{2} N_n q_s, \tag{4}$$

where $\Delta\chi$ is the electronegativity difference of the two species occupying the two sublattices and κ is the average value of κ_{Cl} and κ_{Na}, where we have indexed κ with the symbols Na and Cl to distinguish the two different species on the sublattice.

The system is positive definite and hence stable if the prefactor to the term quadratic in q_s is positive, i.e., when

$$N_n \kappa_s + 2\kappa N_n^2 - \frac{\alpha_M}{\pi\epsilon_0} \frac{N_n^2}{a} > 0 \tag{5}$$

in which case v can be minimized by requiring that $\partial v / \partial q_s$ vanishes and thus

$$Q = \pm \frac{N_n^2 \Delta\chi}{N_n \kappa_s + 2\kappa N_n^2 - \frac{\alpha_M}{\pi\epsilon_0} \frac{N_n^2}{a}}. \tag{6}$$

Generalization to other two-atomic crystals remains relatively simple as long as each atom has a well-defined position in the unit cell so that Madelung constants can be defined.

B. Notation and convention

In this section, we will define some of the notations and conventions used throughout the remainder of the paper. Lattice points will be indexed with three indices (l,m,n) such that

$$\frac{1}{a}\mathbf{R}_{lmn} = l\mathbf{e}_x + m\mathbf{e}_y + n\mathbf{e}_z \tag{7}$$

when they are explicitly indexed. Unless mentioned otherwise, indices l, m, and n will run from one to N_x, N_y, and N_z, respectively, which will be taken to be infinity in the analytical calculations.

The split charge flown from atom $(l+1)mn$ to atom lmn will be denoted as $q^{(1)}_{lmn}$, and likewise the split charge flown from atom $l(m+1)n$ to lmn will be denoted as $q^{(2)}_{lmn}$, etc. With this notation the charge on atom lmn can be written as

$$Q_{lmn} = q^{(1)}_{lmn} - q^{(1)}_{(l-1)mn} + q^{(2)}_{lmn} - q^{(2)}_{l(m-1)n} + q^{(3)}_{lmn} - q^{(3)}_{lm(n-1)}. \tag{8}$$

This notation will allow us to map the diagonalization procedure of the split-charge formalism onto an eigenmode problem of lattice vibrations in the simple cubic (or rocksalt) crystals. Please note that this mapping is not critical to the results but a matter of rather large convenience.

The assumption of the continuum limit in the SQE model is that the q_{lmn} are smooth functions of their indices so that it is meaningful to define continuous functions $q(\mathbf{R})$ reflecting the split charges at the lattice sites. Interpreting Eq. (8) as a finite difference version of a gradient, one can also describe charges as smooth functions of $\mathbf{R}$ via

$$Q(\mathbf{R}) = a\partial_\alpha q_\alpha(\mathbf{R}). \tag{9}$$

Note that $Q(\mathbf{R})/a^3$ corresponds to the charge density, $\rho(\mathbf{R})$; i.e., $Q(\mathbf{R})$ is the charge contained in an appropriately chosen elementary cell around a given lattice point.

In reciprocal space, Eq. (9) reads as

$$\tilde{Q}(\mathbf{k}) = iak_\alpha \tilde{q}_\alpha(\mathbf{k}) \tag{10}$$

in the continuum limit, where we have assumed the summation convention over identical Greek indices. For lattices other than simple orthorhombic lattices, explicit summation would be required because the orientation of the split charges would not align any longer with the Cartesian coordinate axis and the continuum limit calculations would be more cumbersome to be carried out.

In analogy to lattice problems, one could associate the $q_\alpha(\mathbf{R})$ as vibrations in the α direction. The κ_s would then correspond to on-site springs, while the κ would reflect springs between two nearest-neighbor particles. These springs would not only have a longitudinal component but also transverse (i.e., bending) components of identical magnitude.

If one wants to take into account the discreteness of the lattice and its periodicity when relating the split-charge field and the charge density, then the term k_α in Eq. (10) should be replaced with the following expression:

$$k_\alpha \to \frac{2}{a}\sin\left(\frac{k_\alpha a}{2}\right). \tag{11}$$

While the lattice constant a was used to define the unit of length, we will formally write the number density of atoms, n, as $n=1/a^3$. In the bulk, there are three split charges per atom on average so that one can define the split-charge density as $n_s=3n$. The number density of the split charge with a given index is the same as the atomic density.

Lastly, we would like to define the prefactors for the Fourier series coefficients;

$$q_\beta(\mathbf{R}) = \sum_{\mathbf{k}} \tilde{q}_\beta(\mathbf{k}) e^{ik_\alpha R_\alpha}, \tag{12a}$$

$$\tilde{q}_\beta(\mathbf{k}) = \frac{1}{N}\sum_{\mathbf{R}} q_\beta(\mathbf{R}) e^{-ik_\alpha R_\alpha}. \tag{12b}$$

The same convention for Fourier transformation will be used for the charges $Q(\mathbf{R})$ and their Fourier transform $\tilde{Q}(\mathbf{k})$. This way $\tilde{Q}(0)$ corresponds to the average charge.

C. Diagonalization of the split-charge energy

In this section, we will express the energy of the split-charge model in reciprocal space. We start by setting up the energy in real space. Realizing that the energy of a split charge in an electrostatic field $\mathbf{E}(\mathbf{R})$ due to *external* charges (not to be confused with external field) is $-q_\alpha(\mathbf{R})E_\alpha(\mathbf{R})$, we can write

$$V = \sum_{\mathbf{R}} \frac{\kappa}{2}Q^2(\mathbf{R}) + \frac{\kappa_s}{2}q_\alpha(\mathbf{R})q_\alpha(\mathbf{R}) - q_\alpha(\mathbf{R})E_\alpha(\mathbf{R}) + \frac{1}{8\pi\epsilon_0}\sum_{\mathbf{R},\mathbf{R}\neq\mathbf{R}'}\frac{Q(\mathbf{R})Q(\mathbf{R}')}{|\mathbf{R}-\mathbf{R}'|}. \tag{13}$$

The last summand is the Coulomb interaction energy, V_C, which can be represented with the help of the Ewald summation. For analytical calculations, it is most convenient to express V_C entirely in reciprocal space. With our convention of the Fourier series and by reducing the $\mathbf{k}$ vectors to those that lie in the first Brillouin zone (BZ) of the simple cubic lattice, we obtain

$$\frac{1}{N}V_C = \frac{1}{4\pi\epsilon_0 a}\sum_{\mathbf{k}\in 1.\mathrm{BZ}} \alpha_M(\mathbf{k}) \tag{14}$$

with

$$\frac{1}{4\pi}\alpha_M(\mathbf{k}) = \lim_{\alpha_E\to\infty} -\frac{\alpha_E}{\sqrt{2\pi}^3} + \sum_{\mathbf{G}} \frac{\exp(-a^2|\mathbf{k}+\mathbf{G}|^2/2\alpha_E^2)}{a^2|\mathbf{k}+\mathbf{G}|^2}, \tag{15}$$

where $\mathbf{G}$ are reciprocal lattice vectors.

Two important limiting cases for our wave-vector-dependent Madelung constant $\alpha_M(\mathbf{k})$ are as follows:

$$\tilde{\alpha}_M(\mathbf{k}) = \begin{cases} 4\pi/(ka)^2 & \text{for } k\to 0 \\ -\alpha_M^{\mathrm{NaCl}} & \text{for } \mathbf{k}=\frac{\pi}{a}(1,1,1) \end{cases}, \tag{16}$$

where $\alpha_M^{\mathrm{NaCl}}=1.748$ is the "regular" Madelung constant for the rocksalt lattice. It is the minimum value of $\alpha_M(\mathbf{k})$ for the simple cubic structure, and hence when the stability condition in Eq. (5) is violated, the system exhibits an instability into the rocksalt structure. More information on the wave vector-dependent Madelung constant can be found in Sec. III.

Doing the Fourier transform on the remaining terms in the SQE potential energy yields

$$\frac{1}{N}V = \sum_{\mathbf{k}} \frac{1}{2}\left(\kappa + \frac{\alpha(\mathbf{k})}{4\pi\epsilon_0 a}\right)\tilde{Q}^*(\mathbf{k})\tilde{Q}(\mathbf{k}) + \frac{1}{2}\kappa_s \tilde{q}_\alpha^*(\mathbf{k})\tilde{q}_\alpha(\mathbf{k}) - \tilde{q}_\alpha^*(\mathbf{k})\tilde{E}_\alpha(\mathbf{k}). \quad (17)$$

Here, it is important to keep in mind that the $\tilde{Q}(\mathbf{k})$ are related to the Fourier coefficients of the split charges via Eqs. (10) and (11). Thus, energy is minimized if

$$\tilde{E}_\alpha(\mathbf{k}) = \{e_{\alpha\beta}(\mathbf{k}) + \kappa_s \delta_{\alpha\beta}\}\tilde{q}_\beta(\mathbf{k}), \quad (18)$$

where

$$e_{\alpha\beta}(\mathbf{k}) = 4\left(\kappa + \frac{\alpha_M(\mathbf{k})}{4\pi\epsilon_0 a}\right)\sin\left(\frac{k_\alpha a}{2}\right)\sin\left(\frac{k_\beta a}{2}\right) \quad (19a)$$

$$\rightarrow \left(\kappa + \frac{1}{\epsilon_0 a}\right)a^2 k_\alpha k_\beta \quad \text{for } k \rightarrow 0. \quad (19b)$$

Thus, one can calculate the response of the split-charge model to a field produced by external charges. It is worth pointing out that the solution is not unique unless $\kappa_s > 0$ as different split-charge distributions can yield the same charge distributions when the bond hardness is zero. It is furthermore worth pointing out that it is instructive to reproduce the stability criterion for the rocksalt lattice from the formalism developed here. The difference in χ_{Na} and χ_{Cl} can be represented by an (added) electrostatic field of magnitude $\Delta\chi/a$ at the wave vector $\mathbf{k}=(\pi/a)(1,1,1)$. Using this wave vector [Eqs. (19) and (18) with the appropriate value of $\alpha(\mathbf{k})$ stated in Eq. (16)], one can see that one will only get a (physically meaningful) positive restoring force on the split charge when Eq. (5) is satisfied.

D. Wavelength-dependent Madelung constant

In this section, we present and discuss the numerical work on the estimation of $\alpha_M(\mathbf{k})$, which we needed to calculate the discretization corrections. The bare data are shown in Fig. 1. The comparison to the continuum limit and the Madelung constant of the rocksalt lattice is successful. However, the range in which the continuum solution is appropriate turns out to be fairly small.

In Fig. 1 we also show the leading-order corrections to the continuum solution. The first symmetry-allowed correction is of order k^2. Including that direction leads to a fair representation of $\alpha(\mathbf{k})$ throughout the first Brillouin zone, although the instability associated with the rocksalt lattice is overestimated slightly. Including the second symmetry-allowed correction leads to essentially quantitative agreement. These terms are the k^4 term, and a term, which is related to the cubic anisotropy, i.e., is the fourth-order cumulant, K_4,

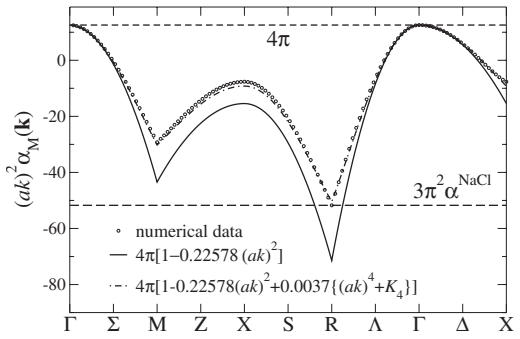

FIG. 1. Wavelength-dependent Madelung constant $\alpha_M(\mathbf{k})$ times the squared wave vector k (in units of the lattice constant a) along selected paths in the first Brillouin zone of the simple cubic lattice. The continuum limit of that expression is 4π, which is shown as the upper dotted line. The value associated with the Madelung constant (times $\pi[1,1,1]$ squared) is represented with the lower straight dashed line. Estimates for the two first leading-order corrections are included as well. K_4 is the fourth-order cumulant defined in Eq. (20).

$$K_4 = -(ka)^4 + \frac{3}{2}\sum_{\alpha=1}^{3}(k_\alpha a)^4. \quad (20)$$

To summarize, $\tilde{\alpha}_M(\mathbf{k})$ can be described rather well throughout the first Brillouin zone in simple cubic and rocksalt structures with the equation

$$\frac{1}{4\pi}\tilde{\alpha}(\mathbf{k}) = 1 - \alpha(ak)^2 + \beta\{(ak)^4 + K_4\}, \quad (21)$$

where $\alpha=0.2257(8)$ and $\beta=0.003(7)$.

E. Dielectric constant and penetration depth

In this section, we will consider a constant electrical field parallel to the z axis and solve the split-charge equations in the continuum limit. From the results, one can calculate the dielectric constant and the penetration depth. To mimic the condition of a periodically continued capacitance geometry, which we use in the simulations (see Sec. III A), we write the electrostatic field on the domain $-(1+\epsilon)z_m < z < (1+\epsilon)z_m$ (with $\epsilon \rightarrow 0$) as

$$\mathbf{E}(\mathbf{R}) = \mathbf{e}_z\{E_0 - E_0 z_m \delta(z \pm [1+\epsilon]z_m)\} \quad (22)$$

and repeat this field along the z direction with period $2z_z$. The presence of the δ functions in Eq. (22) turns the external electrostatic potential into a function that is periodic in space and allows for a direct comparison with the numerical solutions of the problem. The Fourier series coefficients of the z component of the E field satisfy

$$\tilde{E}_3(\mathbf{k}) = \begin{cases} -2E_0, & k_x = k_y = 0,\ k_z = \frac{2\pi n}{(1+\epsilon)z_m},\ n \in \mathbb{N} \\ 0, & \text{else.} \end{cases} \quad (23)$$

Assuming the continuum limit allows one to rewrite Eq. (18) as

$$\tilde{E}_\alpha = \left\{ \left(\kappa a^2 k^2 + \frac{1}{\epsilon_0 a} \right) \frac{k_\alpha k_\beta}{k^2} + \kappa_s \delta_{\alpha\beta} \right\} \tilde{q}_\beta \tag{24}$$

for the given wave vector of interest. Assuming the capacitor geometry described in the precedent paragraph, we can choose $\tilde{E}_\alpha(\mathbf{k}) = -2E_0 \delta_{k_1 0} \delta_{k_2 0} \delta_{3\alpha}$, $k_\alpha = k\delta_{3\alpha}$, and $\tilde{q}_\alpha = \tilde{q}_s \delta_{3\alpha}$ and one can invert this last (matrix) equation to yield

$$\tilde{q}_s(k) = \frac{-2E_0}{\kappa a^2 k^2 + \frac{1}{\epsilon_0 a} + \kappa_s}. \tag{25}$$

Thus, for $k \to 0$, the term related to κ disappears with k^2, which means that there is no restoring force to an external electrostatic field and charge flows until the external electrostatic field is compensated by the polarization charge; i.e., the system behaves as metallic.

The macroscopic or long-wavelength response in the presence of a finite bond hardness (dielectric) divided by that of the metal ($\kappa_s = 0$) is

$$\frac{\tilde{q}_{s,\text{dielectric}}}{\tilde{q}_{s,\text{metallic}}} = \frac{1/\epsilon_0 a}{\kappa_s + 1/\epsilon_0 a} \tag{26}$$

for small k. In the absence of periodic boundary conditions, i.e., for real capacitor geometries, this ratio expresses the percentage of the external field that is annihilated by the polarization response of the system, which is complete annihilation for $\kappa_s = 0$, and thus

$$\epsilon_\mathbf{r} = 1 + \frac{1}{\epsilon_0 a \kappa_s}. \tag{27}$$

When solving the response of the dielectric with given $E_3(z)$, solutions would be obtained by finding the roots in the denominator of Eq. (25). These roots are

$$ak_{1,2} = \pm i \sqrt{\frac{1}{\kappa} \left(\kappa_s + \frac{1}{\epsilon_0 a} \right)}. \tag{28}$$

The absolute values of these roots are an inverse lengthscale, which can be associated with a correlation or penetration depth, δ, for which we thus find

$$\delta = a \cdot \sqrt{\frac{\epsilon_0 a \kappa}{1 + \epsilon_0 a \kappa_s}}. \tag{29}$$

Equations (28) and (29) allow one to choose effective values for the "free" parameters of the SQE model to best reflect the dielectric properties of a given material. Since ϵ_r is "fixed" by the choice of κ_s, the δ can be used to "fine-tune" effective values for κ. Embedding a more specific behavior into the SQE model, such as different functional forms of the dispersion, would require the introduction of split charges beyond nearest-neighbor split charges.

F. Discretization corrections

As can be seen in Sec. II D, the range in which the continuum approximation describes the wave vector-dependent Madelung constant $\alpha_M(\mathbf{k})$ accurately is rather limited. When the first correction is included, it is still relatively simple to solve the continuum model, and at the same time, $\alpha_M(\mathbf{k})$ is obtained quite accurately in a fair fraction of the first Brillouin zone. To include the corrections, we use

$$\alpha_M(k) = 4\pi[1 - \alpha(ak)^2], \tag{30}$$

where $\alpha \approx 0.225\,78$ for the simple cubic lattice.

One can proceed as in Sec. I, except that Eq. (24) is replaced with

$$\tilde{E}_\alpha = \left\{ \left(\kappa a^2 k^2 + \frac{1 - \alpha(ak)^2}{\epsilon_0 a} \right) \frac{k_\alpha k_\beta}{k^2} + \kappa_s \delta_{\alpha\beta} \right\} \tilde{q}_\beta. \tag{31}$$

The roots in the prefactor to $\tilde{q}_\beta$ in this equation from which the penetration depths was calculated are now

$$\delta = a \cdot \sqrt{\frac{\epsilon_0 a \kappa - \alpha}{1 + \epsilon_0 a \kappa_s}}, \tag{32}$$

and thus discretization corrections reduce the penetration depth, which will be particularly apparent when κ is very small.

When κ is sufficiently small, the penetration depth becomes imaginary. For small κ, the values for κ_s must be sufficiently large to guarantee the stability of the dielectric. In that case, the denominator on the r.h.s. of Eq. (25) does not tend to have poles in the first Brillouin zone, which means that the ratio of $\tilde{q}_s(k)$ and $\tilde{E}(k)$ is essentially constant. This in turn implies that for the capacitor geometry considered here, split charges are almost constant through the material; that is, charge only builds up in the last layer on the surface.

III. COMPARISON TO NUMERICAL SOLUTIONS OF THE SQE MODEL

A. Model system and method

In our numerical calculations, we consider a simple cubic lattice of SQE charges. The distance between nearest neighbors, a, is used to define the unit of length; i.e., $a = 1$. This means that the atomic number density of the simple lattice $n = 1/a^3$ and consequently a number density of split charges of $n_s = 3n$. The solids in our calculation are typically composed of $10 \times 10 \times 100$ atoms. While the numerical solutions could have been simplified substantially, e.g., by making use of the fact that the atomic charges in each layer are identical, we felt it was sufficient to use our house-written, "not-special-purpose" molecular-dynamics code.

Periodic boundary conditions are invoked in all three spatial dimensions. The size of the simulation box is $10a \times 10a \times (100 + \epsilon)\ a$; that is, we investigate a sandwich structure with the sandwich normal parallel to the z direction. The extramargin in the z direction breaks the bonds between different periodic images; thus, there are no split charges across the boundary in the z direction. There are two reasons why we chose the dimension parallel to z only marginally larger than the actual crystal. It reduces the computational time, but more importantly, it also appears to reduce finite-size effects. In another set of simulation, i.e., whenever we want to as-

certain the external field, the length of the vacuum slab was increased to that of the dielectric.

As the potential V is bilinear in the split charges, we can use molecular dynamics on them within an extended Lagrangian scheme to find their optimum values. For this purpose, the split charges are assigned a mass $m_{ij}=\kappa_{ij}+\kappa_i+\kappa_j$, which moves the characteristic frequency of an oscillation to roughly unity. The equations of motion are damped with a term $-m_{ij}\gamma\dot{q}_{ij}$, where the damping constant is typically chosen to be 1/2. This choice for γ renders the motion to be very slightly underdamped. The molecular-dynamics time step is chosen to be $\Delta t=2\pi/20$ so that one typical oscillation is decomposed into 20 time steps. (For large ratios of κ/κ_s smaller dampings are preferential to avoid overdamping of long-wavelength modes.) For calculations, where κ is similar to or larger than κ_s, the system is essentially relaxed after 20 time steps; for smaller ratios, more time steps have to be carried out.

B. Results

In this section, we will test the analytical predictions with the numerical solutions of the model system that is described in Sec. II. We start the test of our analytical results by comparing a measurement of the penetration depth from simulations to those obtained in the regular continuum solution. The equation for the penetration depth is given in Eq. (29), and from this equation, one can find the spatial or z dependence to be

$$\rho(z) \propto \sinh(z/\delta), \tag{33}$$

where we could make use of the problem's symmetry by placing the center of mass of the simulation cell into the origin of the coordinate system; i.e., the charges decay exponentially into the system from both surfaces at a rate proportional to $1/\delta$. In Fig. 2 we demonstrate that this prediction is accurate within symbol size, at least for the investigated value of $\delta=10a$. Three cases are shown explicitly: one metal ($\kappa_s=0$), one dielectric with an extremely small polarizability ($\kappa_s=200$), and one case in between. As the continuum solution becomes better with increasing δ one can state that the continuum solution is applicable for $\delta \geq 10a$.

Next, we want to test the equation for the dielectric constant, i.e., Eq. (27). To do this, the electrostatic field is measured inside the solid at atomic sites (neglecting the on-site charge) and at the vertex points of the elementary cells, where the contribution of eight nearest identical charges would cancel exactly. The atomic-site value and the average of the eight vertex points are averaged, which gives a fair estimate of the electrostatic field in one elementary cell. Unfortunately, we cannot simply associate the external field with the externally applied electrostatic field. The reason is that due to the periodic boundary conditions, it is not defined if the vacuum slab or the dielectric slab is within the capacitance. In other words, surface effects prevail in an infinitely repeated array of capacitances. In order to yet determine the external field we increased the vacuum slab and calculated the electrostatic field with the same (Ewald summation) subroutines as those that were used to produce the charges.

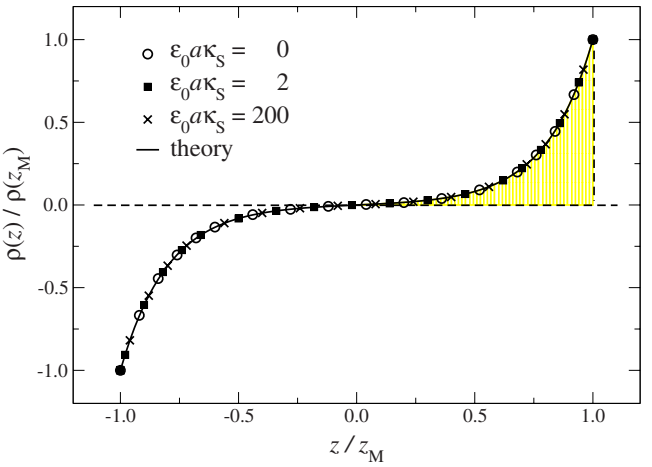

FIG. 2. (Color online) Comparison of numerical data and theory on the z dependence of the charge density. In the calculations, the number of layers was 100, and thus $z_M=50a$. κ was chosen such that the penetration depth $\delta=10a$ remained constant, which makes the normalized charge density $\rho(z)/\rho(z_M)$ collapse onto a single curve. The shaded area reflects the (normalized) surface charge from the continuum limit treatment. There is no adjustable coefficient in the theory.

Changing the cutoffs in real and reciprocal states did not alter the results. Some data of the z dependence on E are shown exemplarily in Fig. 3. It can be shown that the electrostatic field remains constant outside the material and decays to another constant value within, which is greater than zero for positive values of κ_s. For $\kappa_s=0$, the total field inside the material decays exponentially, mimicking the response of an ideal conductor.

In order to measure ϵ_r, the dielectric constant, we use the equation

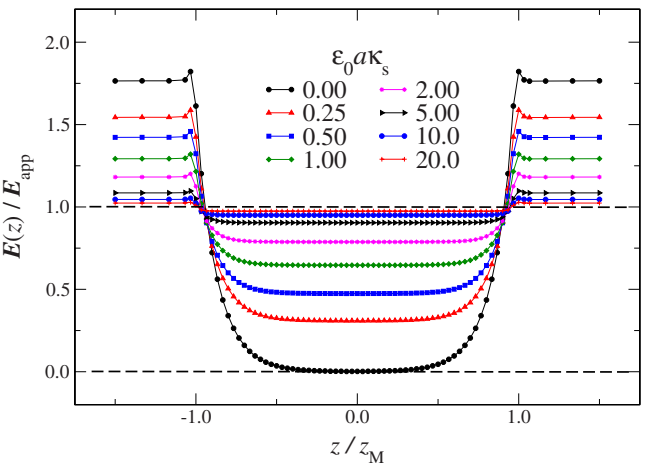

FIG. 3. (Color online) Normalized z component of the electrostatic field in the capacitor geometry as a function of z (normalized on half the thickness, z_M, of the dielectric) for different values of κ_s. Here, the bulk capacitor material is $N_z=60$ layers thick and placed in a simulation box $2N_z a$ units long. The system is subjected to a constant externally applied field oriented along the z axis with magnitude E_{app}. The atomic hardness of the material is fixed at $\epsilon_0 a\kappa=4$.

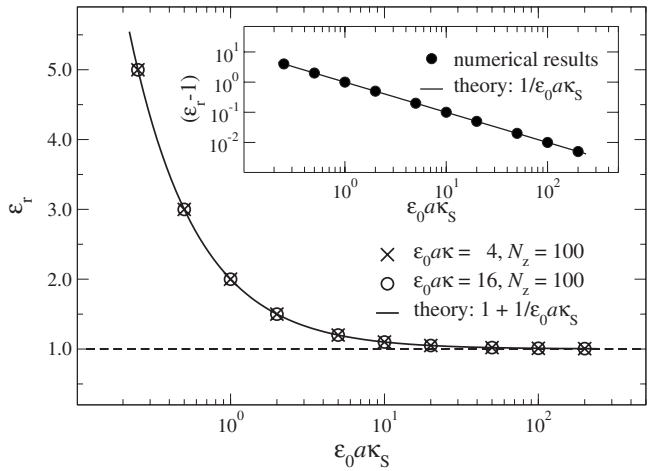

FIG. 4. Dielectric constant ϵ_r as a function of κ_s for two different values of κ. The inset shows the same data as the main figure but on a shifted lin-log graph.

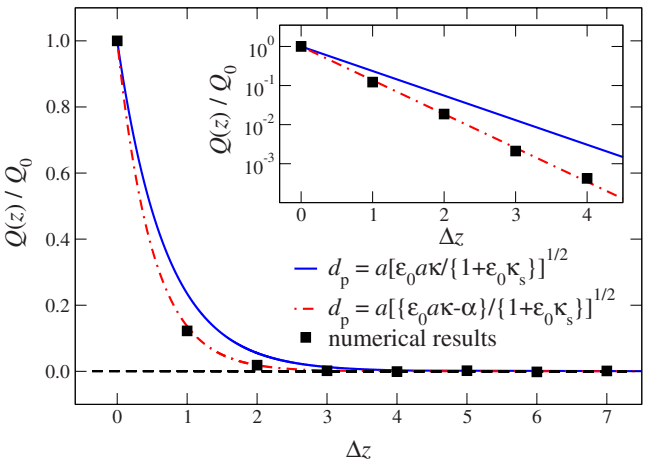

FIG. 5. (Color online) Atomic charges near the surfaces as a function of the distance from the surface, where the surface is located at $\Delta z=0$. Squares are numerical data. Long-dashed (red) and solid (blue) lines represent the predictions by the continuum treatment with and without corrections. The inset is a linear-logarithmic plot of the main figure. In the data shown, $\epsilon_0 a\kappa=3/2\pi$ and $\kappa_s=0$, which is close to the point at which the dielectric response becomes unstable.

$$\epsilon_r E_{\text{int}} = E_{\text{out}}. \tag{34}$$

The ratio $E_{\text{int}}/E_{\text{out}}$ is determined from data that are shown in Fig. 3 and from related data. Results for ϵ_r are shown in Fig. 4. The error between simulation and prediction was less than 0.1% in all cases investigated, where $\kappa_s > 0$. It could always be reduced by reducing the controllable errors in the numerical calculations, such as by increasing the system size, improving the cutoffs in the Ewald summation, or relaxing the system for a longer time, providing evidence that Eq. (27) is exact.

Lastly, we wish to demonstrate that the dispersion or finite discretization correction to the Madelung constant can be used to improve the spatial variation of the electrostatic field. This is done in Fig. 5, where the charge density of a conductor with small penetration depth δ is shown. For the selected parameters, the regular continuum treatment overestimates δ by almost 50% while, including the corrections to $\alpha(\mathbf{k})$ up to second order, reduces the error to less than 1 % for the chosen parameters. Numerical errors, in particular due to the Ewald summation, become relevant when the induced charges are very small, which is apparent in the linear-logarithmic representation. However, as before, errors are controllable by increasing the cutoffs, relaxation times, etc.

IV. DISCUSSION AND CONCLUSIONS

In this paper, we used continuum theory and numerical methods to investigate the dielectric properties of the split-charge formalism, which contains the regular charge equilibration method as a limiting case when the bond hardness is set to zero. In the other limit, i.e., when the atomic hardness is set to zero, SQE corresponds to pure bond-type charge equilibration approaches. For systems that can be described as simple cubic or rocksalt structures we find that the dielectric constant follows the equation

$$\epsilon_r = 1 + \frac{n_s}{9\epsilon_0 \alpha_s}, \tag{35}$$

where we have rewritten Eq. (27) by introducing the term $\alpha_s = \kappa_s a^2$, which is the (dipole) polarizability associated with a split charge and where we expressed the split-charge density n_s as $3/a^3$. Equation (35) has the same structure as a truncated density expansion of the Clausius Mossotti relation; see Ref. 17 for a pedagogical derivation of that relation. However, for the split-charge model, the expansion truncates after the first-order term in density. An interesting consequence of Eq. (35) is that the dielectric constant diverges in the limit of zero bond stiffness, which implies that regular charge equilibration methods produce the same electrostatic fields as metals.

Besides predicting correctly the dielectric constant as a function of the microscopic parameters of the SQE model, we also find that the penetration depth is predicted correctly by the continuum approach, although discretization corrections are required when the characteristic length scales approach values in the vicinity of the lattice constant. Another feature that corrections to the continuum solutions capture correctly, at least for simple cubic systems, is the point in the Brillouin zone where the dielectric response first shows instability upon a decrease in lattice constant; i.e., the system becomes unstable at the largest reciprocal lattice vector contained in the first Brillouin zone. Such instabilities are often deemed as unphysical, but solid H_2, for example, becomes infrared active under high pressure.[18] That situation, if rationalized within an SQE model, would require restoring terms that couple to the fourth moments of split or net charges, and it might be worth pursuing these higher-order terms for systems under large pressure.

An appealing property of the split-charge method is that the "adjustable" parameters can be parametrized directly from experiments. The dielectric constant (at least its high-frequency/electronic part) translates directly into a value for κ_s, and the atomic hardnesses follow from atomic data for electronegativity and ionization energy. Alternatively, one may want to use a value for κ that best reflects the penetra-

tion depth on which the external electrostatic field decays to the value inside the solid.

It is difficult to speculate how much the SQE model can improve existing force fields, in particular, how much better electrostatic interactions will be modeled near surfaces as compared to, for example, current implementation of the regular QE approach in CHARMM (Ref. 19) or REAX force field.[20] However, given the results in the original SQE work,[15] it seems as though its advantages are particularly strong when two chemical moieties are in close vicinity, e.g., the electrostatic potential (ESP) surface of a water methane dimer was found to have an error of 59% with regular QE, which was reduced to 29% with SQE. Of course, when electrostatic field lines are parallel to a dielectric surface, much further improvement is to be expected because the regular QE model behaves like a metal and thus excludes these transverse components, while SQE has the ability to mimic dielectrics.

One challenge that the SQE model will certainly face in molecular-dynamics simulations is that extended Lagrangian schemes are not straightforwardly applicable when κ_s diverges during bond breaking. A large κ_s will induce high-frequency oscillations unless the "split-charge mass" was made time dependent and adjusted according to changes in κ_s. Thus, we expect future implementations of the SQE method into simulation software to be based on regular minimization techniques.

We would like to summarize our discussion by formulating a list of requirements for charge-transfer potentials. They should have the following features: (i) adjustable dielectric constant, (ii) adjustable penetration depth of the electrostatic field, (iii) retain, at least in principle, the parametrization of κ and χ from atomic principles, (iv) produce the correct dissociation limit for broken chemical bonds without invoking externally imposed charge neutrality constraints, and show the correct scaling of the polarizability with the degree of polymerization for polymer chains in the limit of (v) long chains and (vi) short chains. Pure atom-based charge equilibration approaches violate (i), (iv), and (v), while pure bond-based charge equilibration approaches (in which the bond hardness diverges when the bond breaks) violate (ii), (iii), and (vi). The split-charge method does not violate any of the criteria, which is why we would argue that it bears great potential for the use in classical force fields. Of course, as argued in, for instance, Ref. 14, it will be necessary to include on-site atomic polarization to also reflect polarization normal to the bonds. Corrections of this type can be added to the split-charge model in the same way as they can be added to regular charge fluctuation models.

ACKNOWLEDGMENTS

M.H.M. acknowledges financial support from the Natural Sciences and Engineering Research Council of Canada and computational resources from SHARCnet.

*http://publish.uwo.ca/~mmuser/; mmuser@uwo.ca

[1] S. W. Rick and S. J. Stuart, Rev. Comput. Chem. **18**, 89 (2002).
[2] J. W. Ponder and D. A. Case, Adv. Protein Chem. **66**, 27 (2003).
[3] S. Patel and C. L. Brooks, Mol. Simul. **32**, 231 (2006).
[4] W. J. Mortier, K. van Genechten, and J. Gasteiger, J. Am. Chem. Soc. **107**, 829 (1985).
[5] A. K. Rappé and W. A. Goddard III, J. Phys. Chem. **95**, 3358 (1991).
[6] R. G. Parr and R. G. Pearson, J. Am. Chem. Soc. **105**, 7512 (1983).
[7] P. Itskowitz and M. L. Berkowitz, J. Phys. Chem. A **101**, 5687 (1997).
[8] R. Chelli, P. Procacci, R. Righini, and S. Califano, J. Chem. Phys. **111**, 8569 (1999).
[9] G. Lee Warren, J. E. Davis, and S. Patel, J. Chem. Phys. **128**, 144110 (2008).
[10] J. Morales and T. J. Martinez, J. Phys. Chem. A **105**, 2842 (2001).
[11] J. Chen and T. J. Martinez, Chem. Phys. Lett. **438**, 315 (2007).
[12] D. Mathieu, J. Chem. Phys. **127**, 224103 (2007).
[13] S. W. Rick, S. J. Stuart, and B. J. Berne, J. Chem. Phys. **101**, 6141 (1994).
[14] H. A. Stern, G. A. Kaminski, J. L. Banks, R. Zhou, B. J. Berne, and R. A. Friesner, J. Phys. Chem. B **103**, 4730 (1999).
[15] R. A. Nistor, J. G. Polihronov, M. H. Müser, and N. J. Mosey, J. Chem. Phys. **125**, 094108 (2006).
[16] R. L. McGreevy and L. Pusztai, Mol. Simul. **1**, 359 (1988).
[17] J. H. Hannay, Eur. J. Phys. **4**, 141 (1983).
[18] M. Hanfland, R. J. Hemley, and H. K. Mao, Phys. Rev. Lett. **70**, 3760 (1993).
[19] S. Patel and C. L. Brooks, J. Comput. Chem. **25**, 1 (2004).
[20] A. C. T. van Duin, S. Dasgupta, F. Lorant, and W. A. Goddard III, J. Phys. Chem. A **105**, 9396 (2001).